scientific reports

Check for updates

OPEN

# Regional pulmonary perfusion, blood volume, and their relationship change in experimental early ARDS

Arnoldo Santos[1,2,3], Gabriel C. Motta-Ribeiro[3,4], Nicolas de Prost[3,5], Mauro R. Tucci[3,6], Tyler J. Wellman[3,7], Marcos F. Vidal Melo[3,8] & Tilo Winkler[3]✉

**Regional pulmonary perfusion (Q) has been investigated using blood volume ($F_b$) imaging as an easier-to-measure surrogate. However, it is unclear if changing pulmonary conditions could affect their relationship. We hypothesized that vascular changes in early acute respiratory distress syndrome (ARDS) affect Q and $F_b$ differently. Five sheep were anesthetized and received lung protective mechanical ventilation for 20 h while endotoxin was continuously infused. Using dynamic $^{18}$F-FDG and $^{13}$NN Positron Emission Tomography (PET), regional $F_b$ and Q were analysed in 30 regions of interest (ROIs) and normalized by tissue content ($F_{bn}$ and $Q_n$, respectively). After 20 h, the lung injury showed characteristics of early ARDS, including gas exchange and lung mechanics. PET images of $F_{bn}$ and $Q_n$ showed substantial differences between baseline and lung injury. Lung injury caused a significant change in the $F_{bn}$-$Q_n$ relationship compared to baseline ($p < 0.001$). The best models at baseline and lung injury were $F_{bn} = 0.32 + 0.690Q_n$ and $F_{bn} = 1.684Q_n - 0.538Q_n^2$, respectively. Endotoxine-associated early ARDS changed the relationship between $F_b$ and Q, shifting from linear to curvilinear. Effects of endotoxin exposure on the vasoactive blood flow regulation were most likely the key factor for this change limiting the quantitative accuracy of $F_b$ imaging as a surrogate for regional Q.**

In healthy lungs, pulmonary perfusion and intravascular blood volume show a vertical gradient resulting from gravitational forces, with higher perfusion and blood volume in dependent regions[1,2]. However, it is unknown if regional perfusion and regional blood volume have a tight constant relationship or if certain conditions such as endotoxin exposure during early acute respiratory distress syndrome (ARDS) may change their relationship due to its effect on vascular properties[3]. Clinically relevant would be for example decreases in the regional blood volume resulting in regional vascular collapse causing alveolar dead space and potentially vascular injury, micro-clotting of the blood, or redistribution of perfusion resulting in a mismatch between ventilation and perfusion and impairment of pulmonary gas exchange.

During ARDS, the evaluation of pulmonary perfusion is particularly relevant[4] because changes in regional perfusion resulting in a mismatch between ventilation and perfusion worsen gas exchange leading to oxygen refractory hypoxemia, one of the landmarks of ARDS. During the early phase of ARDS, alterations in the regional conditions including inflammation, vasoconstriction or -dilation, blood clotting, alveolar overdistension, and the intravascular-to-alveolar pressure difference can change the perfusion distribution in the lungs. Furthermore, the effects of these factors can be enhanced by the alveolar pressure changes mediated by mechanical ventilation. Besides the effect on gas exchange, changes in pulmonary vascular resistance (PVR) during ARDS can have a clinically significant effect on right ventricular (RV) failure that has been demonstrated to affect patient outcomes[5].

[1]Intensive Care Medicine Department, Hospital Universitario Fundación Jiménez Díaz, IIS-FJD, Madrid, Spain. [2]CIBER de enfermedades respiratorias CIBERES ISCIII, Madrid, Spain. [3]Department of Anesthesia, Critical Care and Pain Medicine, Massachusetts General Hospital and Harvard Medical School, Boston, MA, USA. [4]Biomedical Engineering Program, Universidade Federal do Rio de Janeiro, Rio de Janeiro, Brazil. [5]Medical Intensive Care Unit, Hôpital Henri Mondor, Assistance Publique - Hôpitaux de Paris, Créteil, France. [6]Divisao de Pneumologia, Faculdade de Medicina, Instituto do Coracao, Hospital Das Clinicas HCFMUSP, Universidade de Sao Paulo, Sao Paulo, SP, Brazil. [7]GE Healthcare, Ultrasound Digital Solutions, San Mateo, CA, USA. [8]Department of Anesthesiology, Columbia University Irving Medical Center, 622 West 168th St., PH 5-505, New York, NY 10032, USA. ✉email: twinkler@mgh.harvard.edu

Dual-energy computed tomography (DECT) allows imaging of perfused blood volume, which has been shown to correlate with regional perfusion[6,7] and its availability and speed may have advantages compared to pulmonary SPECT, PET, and CT perfusion imaging methods, e.g. Refs.[6,8–13]. However, it remains unclear if the relationship between regional blood volume and perfusion could change. For example, it has been shown that hypoxic pulmonary vasoconstriction (HPV) is severely blunted in acute lung injury[12], and regional changes in vasoactive blood flow regulation could affect the relationship between blood volume and perfusion. Also, a PET imaging study reported a curvilinear relationship between blood volume and perfusion in humans[13]. If the relationship between blood volume and perfusion is not linear and/or changes in the presence of lung injury, imaging regional blood volume as a surrogate for perfusion could be inaccurate.

A model that resembles major changes caused by ARDS in lung vasculature is that caused by intravenous lipopolysaccharide infusion[3,14,15]. It has been described that endotoxine-associated early ARDS causes an increase in pulmonary vascular resistance and a decrease in pulmonary vascular compliance. The combined effect on these vascular properties could lead to a modification in local pulmonary perfusion as well as in local blood volume, particularly in presence of pulmonary heterogeneity as seen in ARDS.

In this study, we hypothesized that lung injury representative of early ARDS with endotoxin exposure is associated with changes in the regional vasoactive blood flow regulation affecting the relationship between blood volume and perfusion. We aimed to study the effects of lung injury on regional perfusion and blood volume in an animal model using PET imaging.

## Material and methods

We performed a detailed new analysis of the regional pulmonary perfusion and blood volume, and changes in their relationship using the original PET imaging data of a previously published experimental study in 6 sheep[16]. One animal could not be included in this analysis due to a technical problem with a PET scan. The Subcommittee on Research Animal Care at the Massachusetts General Hospital approved the experimental protocols. All methods were performed in accordance with the relevant guidelines and regulations. This study is reported in accordance with ARRIVE guidelines.

### Subjects and experimental design

The experimental design has been previously described in detail[16]. Briefly, sheep were anesthetized, intubated and mechanically ventilated using volume control, positive end-expiratory pressure (PEEP) 5 cm $H_2O$, tidal volume 6 ml/kg, inspired $O_2$ fraction ($FiO_2$) to maintain an arterial oxygen saturation ≥ 90% and respiratory rate to keep the arterial $CO_2$ pressure ($PaCO_2$) between 32 and 45 mmHg. Further details are described in the online supplement.

Once animal instrumentation was completed, baseline measurements of physiological parameters were obtained. Subsequently, a set of dynamic $^{13}$NN and $^{18}$F-FDG PET images was acquired.

After baseline (BL) measurements, animals were subjected to a continuous lipopolysaccharide (*Escherichia coli* O5:55, List Biologic Laboratories Inc, USA) infusion of 10 ng/kg/min for 20 h to induce lung injury[16]. Then measurements were repeated for lung injury (INJ). During the time of the experiment, PEEP and $FiO_2$ were managed according to the ARDS Network table (low PEEP high $FiO_2$)[17].

### PET image acquisition

The PET imaging equipment, protocol, and processing methods have been previously presented in detail[11,18–20], and are described in the online supplement. Briefly, we collected 15 PET transverse adjoining slices of 6.5-mm thickness, estimated to encompass approximately 70% of the total sheep lung volume. Reconstructed images consisted of an interpolated matrix of 128 × 128 × 15 voxels with a size of 2.0 × 2.0 × 6.5 mm each. Three different types of PET images were acquired.

1. Transmission scans were obtained at baseline and at 20 h using a rotating pin source of $^{68}$Ge for 10 min. Transmission scans were used for the attenuation correction of the corresponding emission scans, to delineate the lung field, and to determine the fraction of gas ($F_{gas}$).
2. $^{13}$NN (nitrogen) emission scans were obtained at baseline and at 20 h for the assessment of regional perfusion ($Q_r$), including shunt using the $^{13}$NN-saline method[20].
3. $^{18}$F-FDG emission scans: after $^{13}$NN clearance, $^{18}$F-FDG dissolved in 8 ml saline (approximately 40 MBq at baseline and 200 MBq at 20 h) was infused at a constant rate through the jugular catheter for 60 s for the assessment of blood volume.

Further details are provided in the online supplement.

### Image analysis

Lung masks were created from transmission and perfusion scans by thresholding and then manually corrected to assure the adequate selection of lungs. The resulting lung masks were divided in the vertical direction using 15 isogravitational planes and in the axial direction using two sections so that we obtained 30 regions of interest (ROI).

The ROI blood volume was determined by fitting the $^{18}$F-FDG kinetics of each individual ROI to the three-compartment Sokoloff model[21]

$$C_{ROI}(t) = F_b C_p(t) + C_e(t) + C_m(t),$$

where $C_{ROI}(t)$ represents the ROI's $^{18}$F-FDG activity in the PET image, $F_b$ the blood fraction, $C_p(t)$ the concentration of FDG in blood plasma, $C_e(t)$ the concentrations in the extravascular compartment serving as substrate pool for hexokinase, and $C_m(t)$ the concentration of phosphorylated FDG[21,22].

The normalized tissue fraction ($F_{tis,n}$) of each ROI was first calculated as tissue fraction of the individual ROIs using

$$F_{tis} = 1 - F_{gas} - F_b,$$

and then normalized by the mean $F_{tis}$ among the ROIs of each individual using

$$F_{tis,n} = F_{tis}/\text{mean}(F_{tis}).$$

The normalized regional perfusion $Q_n$ of each ROI was first calculated as regional perfusion $Q_r$ equal to the plateau of the $^{13}$NN activity reached at the end of the 60 s breathhold (see online supplement) plus the shunt fraction equal to the relative height of a peak prior to the plateau, and then normalized by the mean perfusion among the ROIs and $F_{tis,n}$.

$$Q_n = Q_r/\text{mean}(Q_r)/F_{tis,n}.$$

So, regional changes in $Q_n$ account for changes in regional lung tissue density. The normalized blood fraction ($F_{bn}$) is based on the blood fraction estimates of the individual ROIs ($F_b$) and normalized by the mean blood fraction among the ROIs and $F_{tis,n}$.

$$F_{bn} = F_b/\text{mean}(F_b)/F_{tis,n},$$

equivalent to the normalization of $Q_n$.

To investigate longitudinal changes in regional perfusion and blood volume accounting for changes in cardiac output (CO) and pulmonary blood volume between the lung injury and baseline conditions, adjusted $Q_n$ ($Q_a$) and $F_{bn}$ ($F_{ba}$) referenced to baseline were calculated using for the lung injury of early ARDS

$$Q_a = Q_n * CO_{INJ}/CO_{BL} \text{ and } F_{ba} = F_{bn} * V_{B,INJ}/V_{B,BL},$$

where $V_B$ is the overall pulmonary blood volume at lung injury ($V_{B,INJ}$) and baseline ($V_{B,BL}$) equal to the sum of the ROIs' products of blood fraction ($F_b$) and mask volume.

For baseline, the adjusted values referenced to baseline are

$$Q_a = Q_n \text{ and}$$

$$F_{ba} = F_{bn}.$$

## Statistical analysis

The primary objective of this study was to determine if the relationship between $F_b$ and Q during lung injury is different from baseline. To answer it, we performed a kernel density estimator (KDE) test under the null hypothesis that the $F_{bn}$ vs $Q_n$ data after lung injury are from the same distribution as the baseline data. As secondary analysis aiming to identify models that describe the relationship between $F_{bn}$ and $Q_n$, we compared six different relationships between $F_{bn}$ and $Q_n$ at baseline and lung injury conditions and the assignment of $F_{bn}$ and $Q_n$ to the independent and dependent parameter using the Bayesian information criterion (BIC) as primary parameter for identifying the best model. Additional details are described in the online supplement.

A p-value $< 0.05$ was assumed as significant. Values are expressed as mean ± standard deviation unless otherwise specified. The effect of endotoxine-associated early ARDS on physiologic variables was evaluated by applying a paired t test. $30 \times 5$ data points were used for the analysis. The computational analysis was performed using Matlab (Mathworks, Natick, MA). The statistical analysis was performed using Stata (v14.2; StataCorp LLC, College Station, TX), the R Statistical Software (v4.2.1)[23], and the ks package (v1.13.5)[24] for the KDE test.

# Results

## Effects of lung injury representative of early ARDS

After 20 h of mechanical ventilation and continuous endotoxin infusion, the animals included in this analysis showed characteristics of lung injury including deterioration in lung mechanics and gas exchange and also an increase in pulmonary vascular resistance (PVR)[16] (Table 1). One animal was excluded from the hemodynamic analysis due to a problem with cardiac output measurement; this also applies for adjustment of $Q_n$ to baseline cardiac output analysis below.

PET images of regional perfusion and blood volume show substantial differences between baseline and lung injury (Fig. 1). The vertical distribution of $Q_n$ among the ROIs shows at baseline a gradual change from dependent (dorsal) to non-dependent (ventral) regions, but it changes during injury to higher perfusion in dependent and less in non-dependent regions compared to baseline (Fig. 1). The vertical distributions of $F_{bn}$ showed a similar distribution.

## The relationship between $F_{bn}$ and $Q_n$ during lung injury representative of early ARDS is different from baseline

Performing a KDE test for the $F_{bn}$-$Q_n$ relationship during lung injury compared to baseline, we found a highly significant difference ($p < 0.001$) showing that the $F_{bn} - Q_n$ point clouds at the two time points are not from the

| Variable | Baseline | Lung injury | p |
|---|---|---|---|
| PEEP ($cmH_2O$) | 6 ± 2 | 10 ± 3 | 0.047 |
| $FiO_2$ | 0.42 ± 0.05 | 0.58 ± 0.21 | 0.120 |
| Tidal volume (ml/kg) | 6.7 ± 0.5 | 7.1 ± 1.1 | 0.487 |
| Plateau pressure ($cmH_2O$) | 14 ± 3 | 23 ± 5 | 0.003 |
| Driving pressure ($cmH_2O$) | 8 ± 2 | 12 ± 2 | 0.006 |
| Respiratory system compliance ($ml/cmH_2O$) | 20.6 ± 4.5 | 13.6 ± 4.1 | 0.034 |
| $PaO_2/FiO_2$ | 342 ± 158 | 185 ± 74 | 0.019 |
| $PaCO_2$ | 46 ± 4 | 43 ± 7 | 0.510 |
| Cardiac output (l/min) | 4.8 ± 0.7 | 3.7 ± 1.1 | 0.187 |
| Mean pulmonary artery pressure (mmHg) | 15 ± 5 | 18 ± 2 | 0.375 |
| Pulmonary vascular resistance ($dyn.s.cm^{-5}$) | 177 ± 57 | 275 ± 34 | 0.006 |

**Table 1.** Physiologic parameters and significance tests of differences.

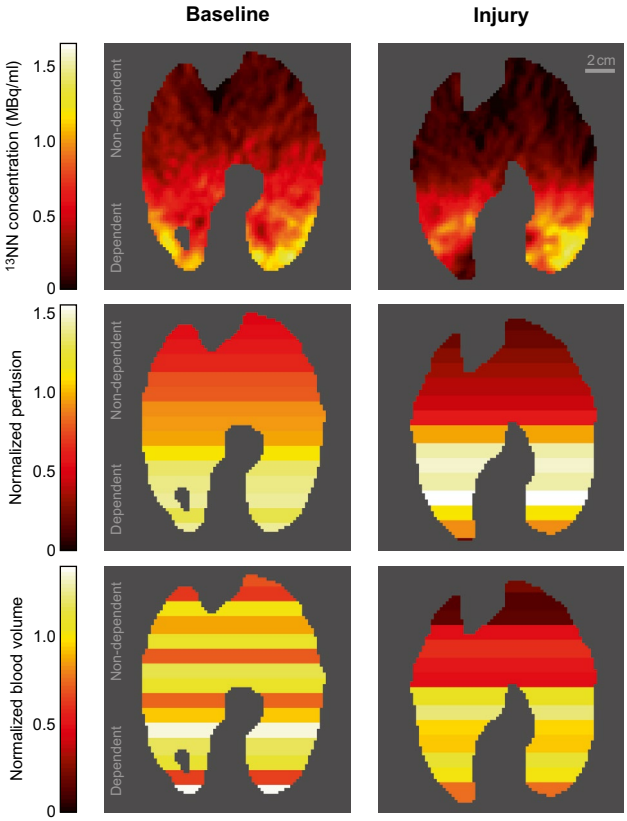


**Figure 1.** Typical slices of $^{13}$NN PET images at baseline and lung injury in supine position. The $^{13}$NN concentration in these images is proportional to the regional perfusion of aerated voxels showing a gradual change along the vertical gradient at baseline. In contrast, lung injury resulted in increased perfusion in the dependent regions and very low perfusion in the non-dependent regions. The normalized perfusion ($Q_n$) of 15 vertically stacked ROIs shows regional differences taking differences in tissue density into account. The distributions of normalized blood volume ($F_{bn}$) correlate with the distributions of normalized perfusion. But the images also illustrate the residual variability of the correlation.

same distribution. After the global test had established this difference, we explored the functional relationships using different mathematical models.

## Characterization of the relationships between $F_{bn}$ and $Q_n$

Using the BIC to compare different models, we identified the linear relationship $F_{bn} = 0.32 + 0.690Q_n$ as the best model for baseline (Fig. 2A, Table 2A). In contrast, the quadratic relationship $F_{bn} = 1.684Q_n - 0.538Q_n^2$ was the best model during lung injury (Fig. 2B, Table 2B). Additionally, a likelihood ratio test comparing linear and

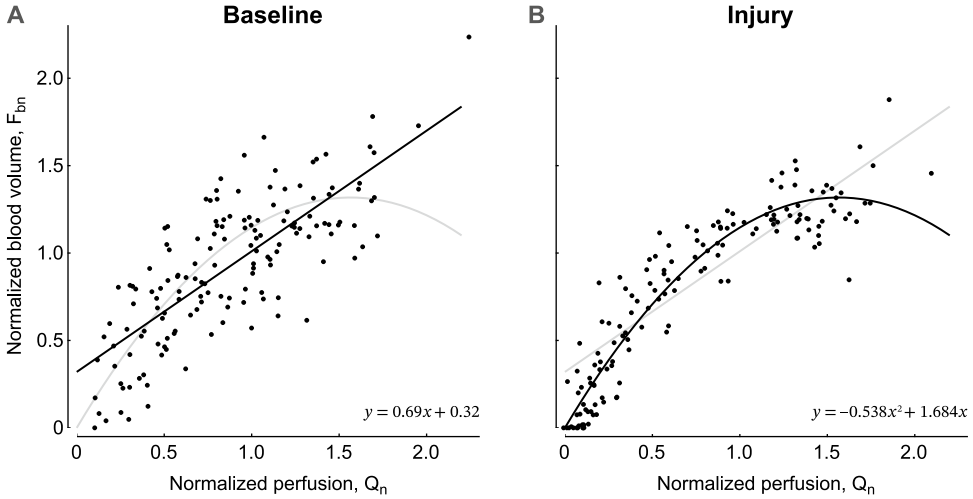


**Figure 2.** Blood volume ($F_{bn}$) vs. perfusion ($Q_n$) of each ROI at baseline (**A**) and lung injury (**B**) show the difference between the two conditions, which a KDE test confirmed as highly significant. Model identification resulted in the selection of a linear relationship as the best model (solid line) for baseline (**A**) and a curvilinear quadratic relationship for lung injury (**B**). Each panel also includes the fitted model of the other condition (grey lines) for reference. Note the difference in the scattering of data points between baseline and lung injury we examined in our discussion. Also, very low perfusion may result in late tracer arrival leading to an underestimation of the blood volume. However, such a bias would not cause a difference between baseline and lung injury.

| Model | a | b | c | BIC |
|---|---|---|---|---|
| A—Baseline | | | | |
| $y = ax$ | 0.980 | | | 62.381 |
| $y = a + bx$ | 0.320 | 0.690 | | 23.977 |
| $y = ax + bx^2$ | 1.433 | − 0.357 | | 27.596 |
| $y = a + bx + cx^2$ | 0.204 | 1.008 | − 0.168 | 25.231 |
| $y = e^{ax}$ | 0.078 | | | 156.465 |
| $y = ae^{bx}$ | 0.503 | 0.650 | | 38.425 |
| B—Lung injury | | | | |
| $y = ax$ | 0.967 | | | 10.437 |
| $y = a + bx$ | 0.214 | 0.780 | | − 30.598 |
| $y = ax + bx^2$ | 1.684 | − 0.538 | | − 106.026 |
| $y = a + bx + cx^2$ | 0.004 | 1.674 | − 0.532 | − 101.042 |
| $y = e^{ax}$ | 0.097 | | | 228.320 |
| $y = ae^{bx}$ | 0.415 | 0.775 | | 38.902 |

**Table 2.** Model comparisons.

quadratic models resulted in chi-square of 3.76 ($p = 0.0526$) for baseline and 76.91 ($p < 0.001$) for lung injury, reinforcing the relevance of quadratic model at early ARDS. The criteria of lowest BIC also suggested better model fitting using $F_b$ as dependent and Q as independent variables than the opposite configuration (online supplement, Table 2A and B). The residual scattering was higher at baseline than lung injury.

## Regional changes in $Q_n$ and $F_{bn}$

In nondependent zones, where $Q_n$ was already low at baseline, the lung injury caused consistently further decreases in perfusion (Fig. 3A). In these zones, the changes in $F_{bn}$ were less consistent, but showed predominantly lower $F_b$ during lung injury than baseline (Fig. 3B). In dependent zones, $F_{bn}$ and $Q_n$ were in most cases higher during injury than baseline, but this effect was more consistent and marked for $Q_n$.

## Relationship of regional changes in adjusted $Q_n$ and $F_{bn}$ referenced to baseline

Although for the most part, changes in the adjusted $Q_n$ and $F_{bn}$ between baseline and injury were similar in direction, the magnitude of these changes for each variable were different and changed according to the vertical gradient (Fig. 4A and B). In the most non-dependent region, decreases in both $Q_a$ and $F_{ba}$ had lower magnitudes than in other regions because they were constrained by their low values at baseline. However, the longitudinal

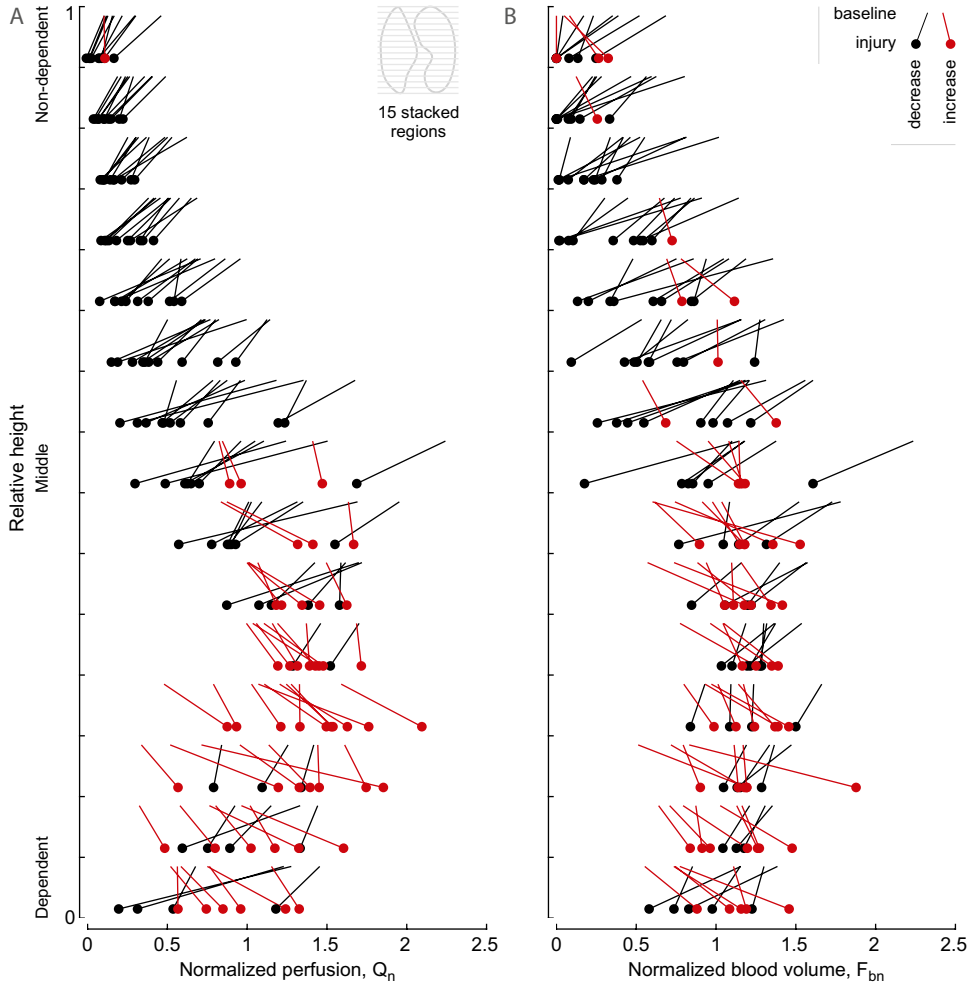


**Figure 3.** Vertical profiles of perfusion ($Q_n$) (**A**) and blood volume ($F_{bn}$) (**B**) with height expressed relative to the lung mask. Changes between baseline and lung injury are visualized as comets within each layer, showing the ROIs of five animals, 150 in total. The profiles and the changes are consistent with the example images in Fig. 1. Note the magnitude and frequency of decreases in perfusion and blood volume in non-dependent regions in contrast to the increases in the dependent half of each profile.

decrease to very low values of both $F_{ba}$ and $Q_a$ demonstrates the very high risk of capillary collapse in the most non-dependent regions in early ARDS with endotoxin exposure. An important insight from comparing regional changes in $Q_a$ and $F_{ba}$ visualized as slopes is the substantial variability in the regional responses rather than a common trend in their longitudinal changes (Fig. 4B).

## Discussion

Using advanced image analysis in an experimental model of lung injury representative of early ARDS with endotoxin exposure, we found that: (1) lung injury affects the relationship between normalized regional blood volume $F_{bn}$ and normalized perfusion $Q_n$, (2) the relationship changed from linear at baseline to curvilinear during lung injury, and (3) changes in the relationship were associated with differences in regional changes in $Q_n$ compared to changes in $F_{bn}$.

These findings are important mainly for the following reasons: (1) They challenge the use of blood volume as a quantitatively accurate surrogate for regional pulmonary perfusion. (2) They suggest that the blood volume-perfusion relationship, rather than being passive like a physical equation, may be affected by vasoactive blood flow regulation, including HPV, blood clotting, pulmonary vascular properties (resistance and compliance) and mechanical ventilation affecting the transmural pressure differences at pulmonary capillaries. (3) They demonstrate regional differentiation in the responses to endotoxin, including relative regional decreases in resistance in dependent regions blunting HPV in contrast to increases in the global PVR, and the risk for a capillary collapse in non-dependent regions.

In human and animal studies, investigators have previously found good correlations between the regional blood volume and perfusion, not normalized by regional differences in tissue fraction, using DECT[6,7] or PET[25,26] for blood volume compared to a perfusion imaging method. These correlations suggested a linear relationship

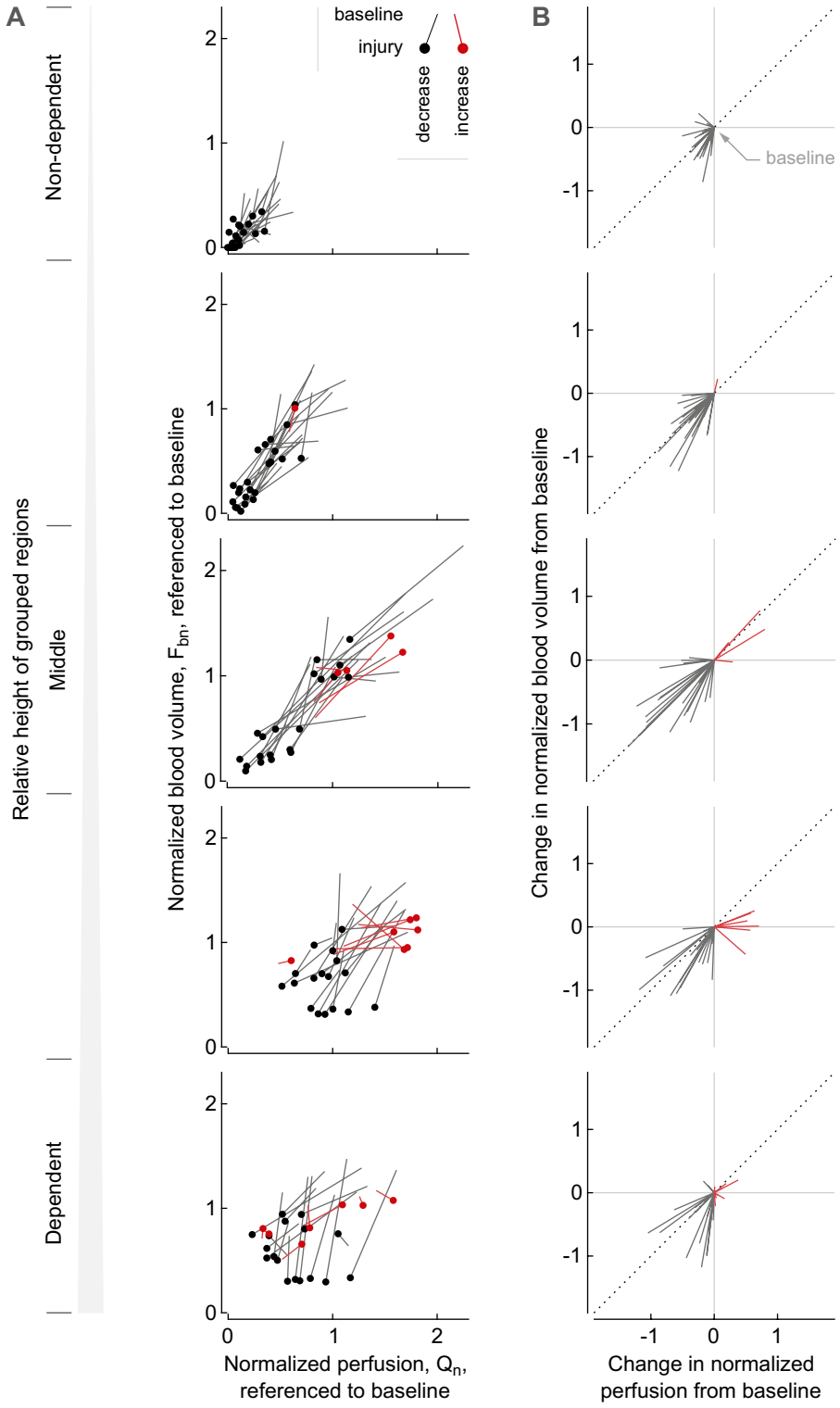


**Figure 4.** Longitudinal changes in normalized perfusion ($Q_n$) and blood volume ($F_{bn}$) between baseline and injury grouped at five levels of relative height show differences in regional responses (**A**), and their changes starting from a common baseline point visualize deviations in Q-Fb relationships (**B**). The longitudinal changes in normalized perfusion and blood volume are referenced to baseline values so that changes in cardiac output and pulmonary blood volume inside the lungs in the field of view are taken into account. The lines represent the ROIs of four animals, 120 in total (one animal was excluded from this visualization due to an unreliable cardiac output measurement). Note the decrease in perfusion and blood volume in non-dependent regions dropping from low to very low or zero (**A**), which constrains the magnitude of the changes from baseline (**B**) and indicates a shift towards regional alveolar dead space. Deviations from the 45-degree slope (dotted line) show that the longitudinal changes in normalized blood volume were not equal to the changes in normalized perfusion.

between the two parameters, which is consistent with the relationship identified in our study at baseline. However, it has not been investigated if lung injury during long-term (20 h) mechanical ventilation with endotoxin exposure may affect this relationship, which has consequences in clinical practice for longitudinal follow-up of changes in patients' lung perfusion. Additionally, a PET study in healthy nonsmoking subjects has shown a curvilinear relationship[13] in contrast to the linear correlations in the studies above.

Regional blood volume imaging relies on perfusion for tracer transport into the blood pool. For longitudinal quantitative assessments of regional changes in perfusion based on blood volume imaging, the relationship between blood volume and perfusion must remain the same when the patient's lung conditions change. However, regional blood flow regulation may not have the same effect on blood volume and perfusion. Additionally, changes in both total perfusion and regional vascular conditions interact with the structure and function of the pulmonary vascular tree such as regional differences in vascular properties, parenchymal tethering, blood clots and local vascular obstructions. We found a significant change in the relationship between blood volume and perfusion between baseline and the lung injury representative of early ARDS in an acute animal model. Besides the changes in vascular properties, such changes in the relationship might also be influenced by the effect of mechanical ventilation. A decrease in lung compliance leads to increased driving pressure, which, added to the necessity of higher PEEP to maintain adequate oxygenation, results in higher plateau pressure. Both higher PEEP and plateau pressure could cause alveoli distension and capillary compression, especially in non-dependent zones.

After a KDE test had established a significant difference between the distributions of $F_{bn} - Q_n$ data at baseline and lung injury, we aimed to identify the best model describing the relationships using BIC. The identified models suggest a linear relationship at baseline and a quadratic relationship at lung injury. The quadratic $F_{bn} - Q_n$ relationship during endotoxin exposure is, despite vasoactive effects of endotoxin, consistent with the behaviour expected of a passive vascular tree. The physical equation for laminar flow suggests that vascular conductance determining the flow has a quadratic relationship with the cross-sectional area of the vessel, and this area is proportional to blood volume if the length of the vessel is equal. A similar curvilinear relationship between perfusion and blood volume has also been found in a PET study in healthy subjects[13]. In contrast, we could not identify a physics-based explanation for the linear relationship at baseline. One plausible explanation for the change in the $F_{bn}$-$Q_n$ relationship from linear at baseline to curvilinear at lung injury could be that regional blood flow regulation in the initially healthy lungs under conditions of anaesthesia at baseline may result in deviations from the physical relationship described above. For example, regional vasoconstriction may cause local obstructions at baseline that are altered by the effects of endotoxin exposure during lung injury, leading to both increased PVR and blunting of HPV[27]. However, regional changes in blood clotting, vascular stiffness, and mechanical ventilation affecting the transmural pressure at pulmonary capillaries could also have contributed to the change.

We speculate that the higher dispersion of residuals relative to the modeled $F_{bn}$-$Q_n$ relationship at baseline compared to lung injury (Fig. 2) is related to the processes that affect the relationship, e.g., regional vasoconstriction. It appears unlikely that the lower $^{18}$F-FDG dose at baseline compared to lung injury, expected to result in higher imaging noise, would affect the blood volume assessment using an FDG kinetics model for ROIs including numerous PET voxels and dynamic PET scans with a substantial number of frames. Furthermore, random errors originating from imaging noise would be expected to result in additional errors symmetrical to the relationship during lung injury using a higher dose, which is not strictly the case.

The higher variations in the $F_{bn} - Q_n$ relationship at baseline may also have increased the residuals during model comparisons to a degree that the BIC of a quadratic model, similar to the relationship for lung injury, lost its advantage over the linear model, which may have contributed to the selection of the linear model for baseline in contrast to the curvilinear model for lung injury representative of early ARDS (Table 2A and B, and online supplement Table 1A). Notably, splitting the overall curvilinear relationship of the lungs into three or more isogravitational ROIs is conceptually similar to a mathematical method called piecewise linear approximation, and results, as expected, in BIC values showing that the linear approximation of the nonlinear relationship during lung injury is sufficient for the individual ROIs with varying slopes and y-intercepts among the ROIs (Online Supplement Table 3).

The distributions of $Q_n$ and $F_{bn}$ over height (Fig. 3) show that regions with low perfusion and low blood volume were located in nondependent areas. Also, $Q_n$ and $F_{bn}$ further decreased in most cases after lung injury, which could lead to capillary collapse. Contributing factors could be the vasoconstrictive effect of endotoxin, increased plateau pressures decreasing the intracapillary-to-alveolar pressure difference, and 'flow stealing' as perfusion shifts to more dependent regions.

Limitations of our study include that we present data from a small sample size which could make it harder to reach a statistical significance. However, we show very consistent characteristics among animals not only at baseline and during lung injury but also for the change from baseline to lung injury. We studied endotoxin infusion as a model of early ARDS which does not represent the entire clinical spectrum of this syndrome. Also, our study is limited to changes during lung injury representative of early ARDS (20 h model) and the relevance or long-term behaviour of our findings are unknown. Nevertheless, the studied period was sufficient to capture changes in $F_{bn}$ and $Q_n$. Finally, the size of ROIs in our study may be larger than in other studies. However, larger ROIs have the advantage that they reduce the random measurement errors by averaging over a larger volume compared to smaller ROIs.

## Conclusions

In an experimental study, endotoxin-associated early ARDS changed the relationship between regional blood volume and perfusion, shifting it from linear to curvilinear. The effects of endotoxin exposure on the vasoactive blood flow regulation were most likely the key factor for this change, suggesting a vasoactive rather than passive

response and limiting the quantitative accuracy of blood volume imaging as a surrogate for regional perfusion and the interpretation of longitudinal changes.

## Data availability

Data are available upon reasonable request. You contact Tilo Winkler (twinkler@mgh.harvard.edu) for this purpose.

Received: 20 June 2023; Accepted: 8 March 2024
Published online: 10 March 2024

## References

1. Musch, G. *et al.* Topographical distribution of pulmonary perfusion and ventilation, assessed by PET in supine and prone humans. *J. Appl. Physiol. (1985)* **93**(5), 1841–51 (2002).
2. Brudin, L. H., Rhodes, C. G., Valind, S. O., Wollmer, P. & Hughes, J. M. Regional lung density and blood volume in nonsmoking and smoking subjects measured by PET. *J. Appl. Physiol. (1985)* **63**(4), 1324–34 (1987).
3. Lambermont, B. *et al.* Analysis of endotoxin effects on the intact pulmonary circulation. *Cardiovasc. Res.* **41**(1), 275–281 (1999).
4. Pelosi, P. & de Abreu, M. G. Acute respiratory distress syndrome: We can't miss regional lung perfusion!. *BMC Anesthesiol.* **15**, 35 (2015).
5. Mekontso Dessap, A. *et al.* Acute cor pulmonale during protective ventilation for acute respiratory distress syndrome: Prevalence, predictors, and clinical impact. *Intensive Care Med.* **42**(5), 862–870 (2016).
6. Fuld, M. K. *et al.* Pulmonary perfused blood volume with dual-energy CT as surrogate for pulmonary perfusion assessed with dynamic multidetector CT. *Radiology* **267**(3), 747–756 (2013).
7. Si-Mohamed, S. *et al.* Head-to-head comparison of lung perfusion with dual-energy CT and SPECT-CT. *Diagn. Interv. Imaging* **101**(5), 299–310 (2020).
8. He, H. *et al.* Influence of overdistension/recruitment induced by high positive end-expiratory pressure on ventilation-perfusion matching assessed by electrical impedance tomography with saline bolus. *Crit. Care* **24**(1), 586 (2020).
9. Borges, J. B. *et al.* Regional lung perfusion estimated by electrical impedance tomography in a piglet model of lung collapse. *J. Appl. Physiol. (1985)* **112**(1), 225–36 (2012).
10. Elojeimy, S., Cruite, I., Bowen, S., Zeng, J. & Vesselle, H. Overview of the novel and improved pulmonary ventilation-perfusion imaging applications in the era of SPECT/CT. *AJR Am. J. Roentgenol.* **207**(6), 1307–1315 (2016).
11. O'Neill, K. *et al.* Modeling kinetics of infused 13NN-saline in acute lung injury. *J. Appl. Physiol. (1985)* **95**(6), 2471–84 (2003).
12. Schuster, D. P., Anderson, C., Kozlowski, J. & Lange, N. Regional pulmonary perfusion in patients with acute pulmonary edema. *J. Nucl. Med.* **43**(7), 863–870 (2002).
13. Brudin, L. H., Rhodes, C. G., Valind, S. O., Jones, T. & Hughes, J. M. Interrelationships between regional blood flow, blood volume, and ventilation in supine humans. *J. Appl. Physiol. (1985)* **76**(3), 1205–10 (1994).
14. Lambermont, B. *et al.* Effects of endotoxic shock on right ventricular systolic function and mechanical efficiency. *Cardiovasc. Res.* **59**(2), 412–418 (2003).
15. Pan, C. *et al.* Low tidal volume protects pulmonary vasomotor function from "second-hit" injury in acute lung injury rats. *Respir. Res.* **13**(1), 77 (2012).
16. Wellman, T. J. *et al.* Lung metabolic activation as an early biomarker of acute respiratory distress syndrome and local gene expression heterogeneity. *Anesthesiology* **125**(5), 992–1004 (2016).
17. Acute Respiratory Distress Syndrome Network *et al.* Ventilation with lower tidal volumes as compared with traditional tidal volumes for acute lung injury and the acute respiratory distress syndrome. *N. Engl. J. Med.* **342**(18), 1301–8 (2000).
18. Musch, G. *et al.* Regional gas exchange and cellular metabolic activity in ventilator-induced lung injury. *Anesthesiology* **106**(4), 723–735 (2007).
19. Musch, G. *et al.* Relation between shunt, aeration, and perfusion in experimental acute lung injury. *Am. J. Respir. Crit. Care Med.* **177**(3), 292–300 (2008).
20. Vidal Melo, M. F. *et al.* Quantification of regional ventilation-perfusion ratios with PET. *J. Nucl. Med.* **44**(12), 1982–1991 (2003).
21. Sokoloff, L. *et al.* The [14C]deoxyglucose method for the measurement of local cerebral glucose utilization: Theory, procedure, and normal values in the conscious and anesthetized albino rat. *J. Neurochem.* **28**(5), 897–916 (1977).
22. Dittrich, A. S. *et al.* Modeling 18F-FDG kinetics during acute lung injury: Experimental data and estimation errors. *PLoS One* **7**(10), e47588 (2012).
23. R Core Team. R: A language and environment for statistical computing. R Foundation for Statistical Computing, Vienna, Austria. https://www.R-project.org/ (2021).
24. Duong T, Wand M, Chacon J, Gramacki A. ks: Kernel Smoothing [Internet], [cited 2022 Aug 22]. https://CRAN.R-project.org/package=ks (2022).
25. Wellman, T. J., Winkler, T. & Vidal Melo, M. F. Modeling of tracer transport delays for improved quantification of regional pulmonary $^{18}$F-FDG kinetics, vascular transit times, and perfusion. *Ann. Biomed. Eng.* **43**(11), 2722–2734 (2015).
26. Pouzot, C. *et al.* Noninvasive quantitative assessment of pulmonary blood flow with 18F-FDG PET. *J. Nucl. Med.* **54**(9), 1653–1660 (2013).
27. Johnson, D., Hurst, T., To, T. & Mayers, I. Interactions of endotoxin, prostaglandins, and circulating cells upon pulmonary vascular resistance. *Circ. Shock* **36**(1), 1–12 (1992).

## Acknowledgements

The authors thank Steve Weise[1] for the expert support with PET imaging and the cyclotron staff John A. Correia[1], Ph.D., and David F. Lee[1], B.S. for the preparation of the radioisotopes. [1]Department of Radiology (Nuclear Medicine and Molecular Imaging), Massachusetts General Hospital, Boston, MA, USA.

## Author contributions

AS and TW conceived the hypothesis and designed the analysis. GCMR contributed to the data analysis. MFVM designed the original experiments, and MFVM, MT, NDP, TJW, and TW performed the animal experiments. AS drafted the manuscript that all authors reviewed, edited, and approved.

## Funding

This work was funded by NIH-NHLBI (National Heart, Lung, and Blood Institute) grant R01-HL121228. GCMR was also funded by CAPES, Ministério da Educação do Brasil (scholarship 6344/15-1).

## Competing interests
The authors declare no competing interests.

## Additional information
**Supplementary Information** The online version contains supplementary material available at https://doi.org/10.1038/s41598-024-56565-6.

**Correspondence** and requests for materials should be addressed to T.W.

**Reprints and permissions information** is available at www.nature.com/reprints.

**Publisher's note** Springer Nature remains neutral with regard to jurisdictional claims in published maps and institutional affiliations.

**Open Access** This article is licensed under a Creative Commons Attribution 4.0 International License, which permits use, sharing, adaptation, distribution and reproduction in any medium or format, as long as you give appropriate credit to the original author(s) and the source, provide a link to the Creative Commons licence, and indicate if changes were made. The images or other third party material in this article are included in the article's Creative Commons licence, unless indicated otherwise in a credit line to the material. If material is not included in the article's Creative Commons licence and your intended use is not permitted by statutory regulation or exceeds the permitted use, you will need to obtain permission directly from the copyright holder. To view a copy of this licence, visit http://creativecommons.org/licenses/by/4.0/.

© The Author(s) 2024